Supporting Information

Heterostructure Design of Mn-Ni(OH)$_2$@1T-MoS$_2$ for Enhanced Aqueous Asymmetric Electrochemical Capacitor

Qingyun Liu [a,*], Yi Wang [b,c], Tianzhao Hu [b,c], Shaorui Chen [b,c], Yaozu Wang [b,c], Hui Zhao [a], Zhigang Yuan [a], Wu Zhang [a], Yulian Wang [a], Zhenhua Sun [b,c], Feng Li [b,c,*]

[a] *School of Materials Science and Engineering, Shenyang Ligong University, Shenyang 110159, China;*

[b] *Shenyang National Laboratory for Materials Science, Institute of Metal Research, Chinese Academy of Sciences, Shenyang 110016, China*

[c] *School of Materials Science and Engineering, University of Science and Technology of China, Hefei 230026, China*

[*]Corresponding author: *qyliu@sylu.edu.cn; fli@imr.ac.cn*

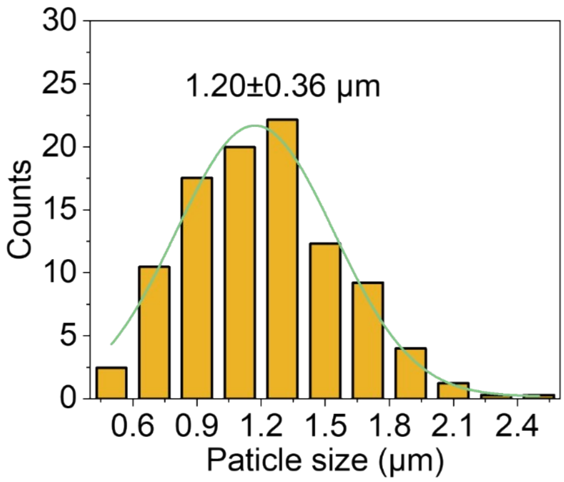

Fig. S1 Particle size distribution histograms of Mn-$Ni(OH)_2$ particles.

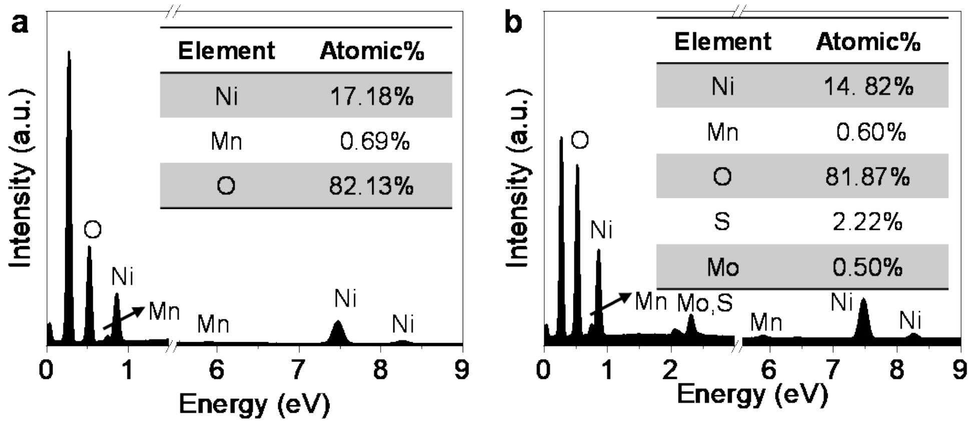

Fig. S2 EDS analysis of (a) Mn-$Ni(OH)_2$ and (b) Mn-$Ni(OH)_2$@1T-MoS_2.

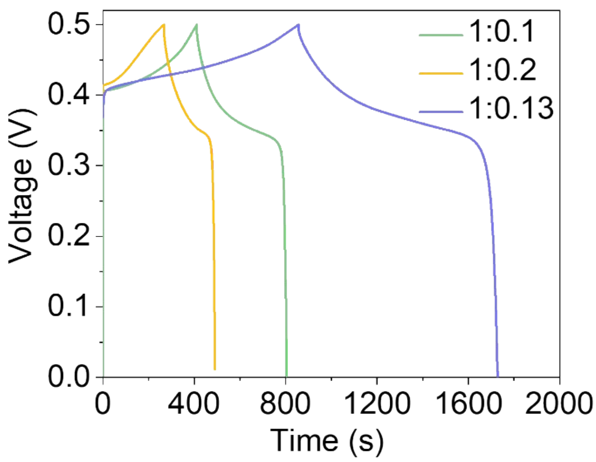

Fig. S3 GCD curves of Mn-Ni$(OH)_2$@1T-MoS_2 with mass ratio of 1:0.1, 1:0.13, and 1:0.2 at 1A g^{-1}.

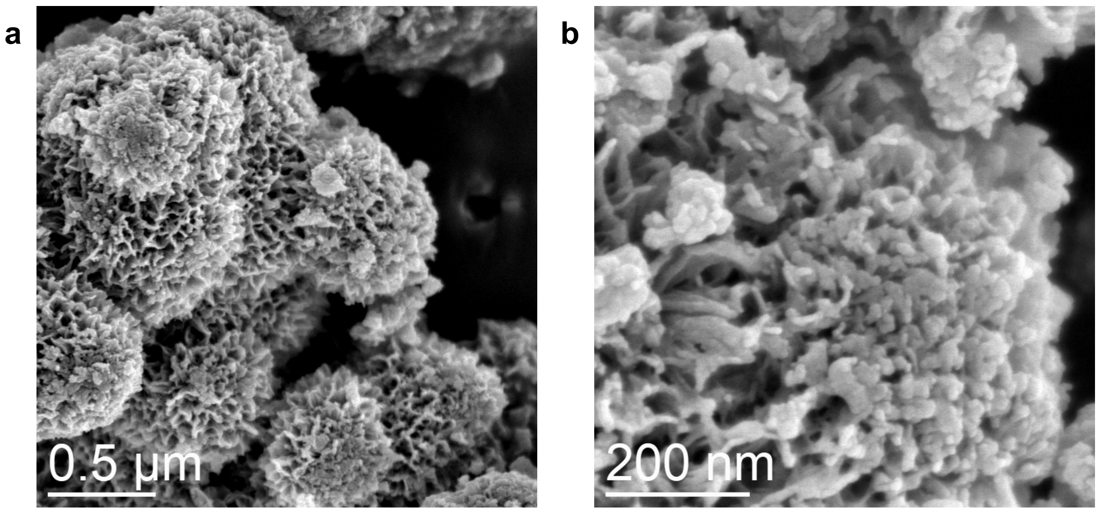

Fig. S4 (a) Low resolution and (b) high resolution SEM images of Mn-Ni$(OH)_2$/1T-MoS_2

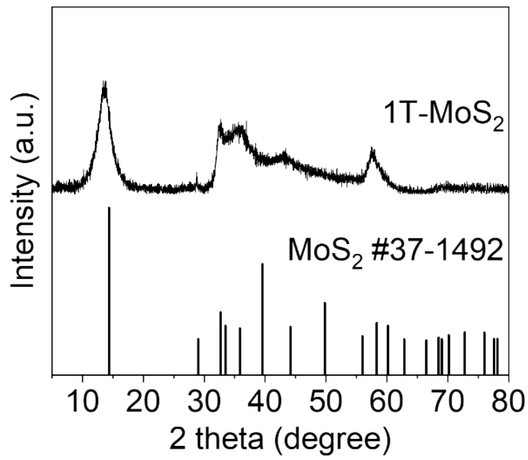

Fig. S5 XRD spectra of 1T-MoS_2 and standard PDF of 2H-MoS_2

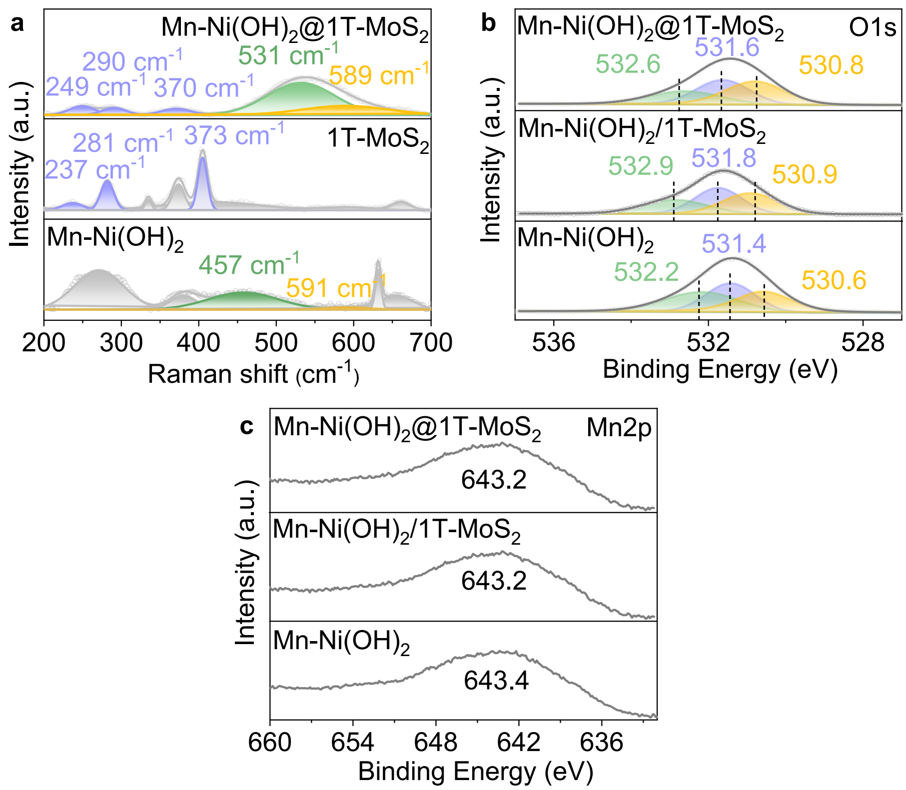

Fig. S6 (a) Raman spectra of Mn-Ni$(OH)_2$@1T-MoS_2; 1T-MoS_2 and Mn-Ni$(OH)_2$ XPS spectra of (b) O 1s and (c) Mn 2p for Mn-Ni$(OH)_2$@1T-MoS_2, Mn-Ni$(OH)_2$/1T-MoS_2 and Mn-Ni$(OH)_2$.

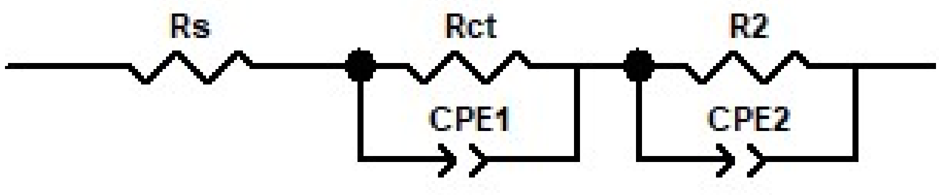

Fig. S7 Equivalent circuit model of Nyquist plots in Fig. 3(a).

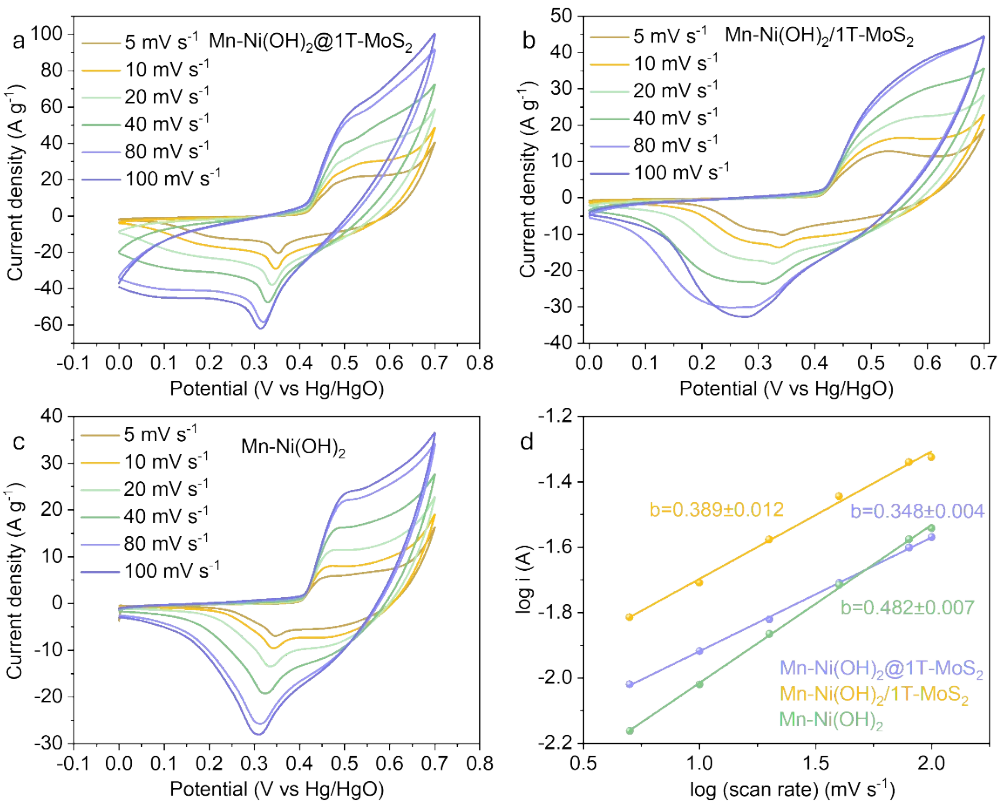

Fig. S8 CV curves of (a) Mn-Ni(OH)$_2$@1T-MoS$_2$, (b) Mn-Ni(OH)$_2$/1T-MoS$_2$, and (c) Mn-Ni(OH)$_2$ electrodes at scan rates ranging from 5 to 100 mV s^{-1}. (d) Relationship of anodic peak currents and scan rates for the as-prepared electrodes.

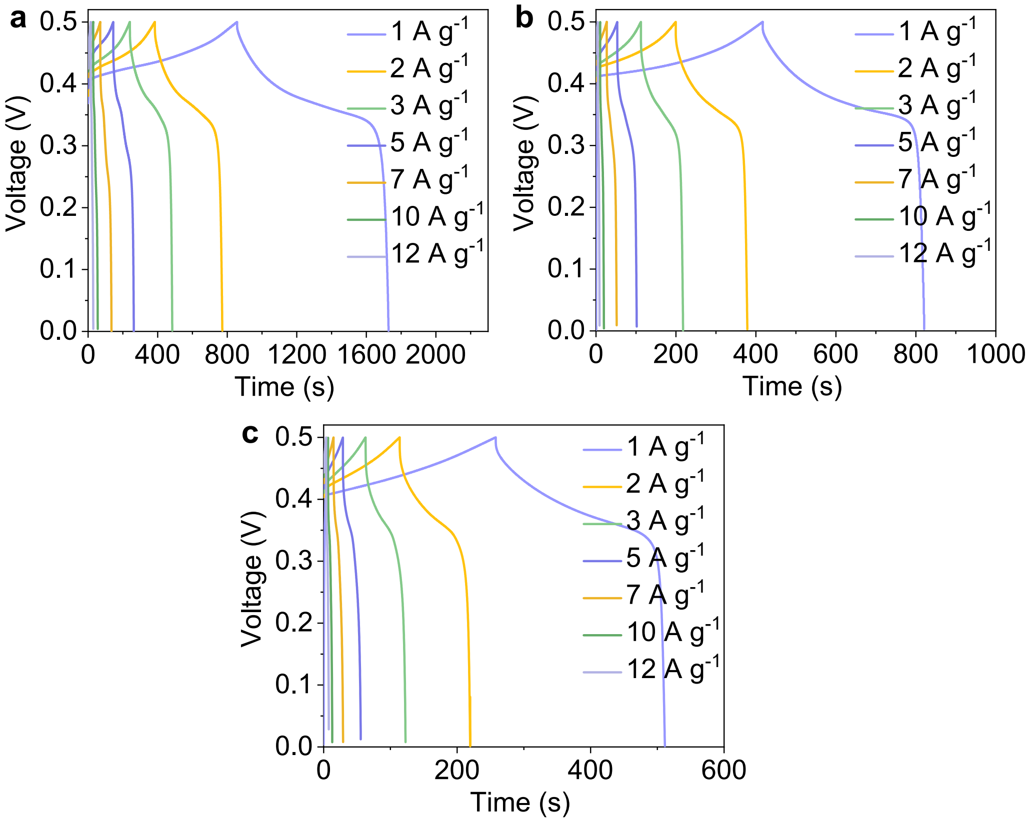

Fig. S9 GCD curves at various current densities from 1 A g^{-1} to 12 A g^{-1} of (a) Mn-$Ni(OH)_2$@1T-MoS_2, (b) Mn-$Ni(OH)_2$/1T-MoS_2 and (c) Mn-$Ni(OH)_2$ electrodes.

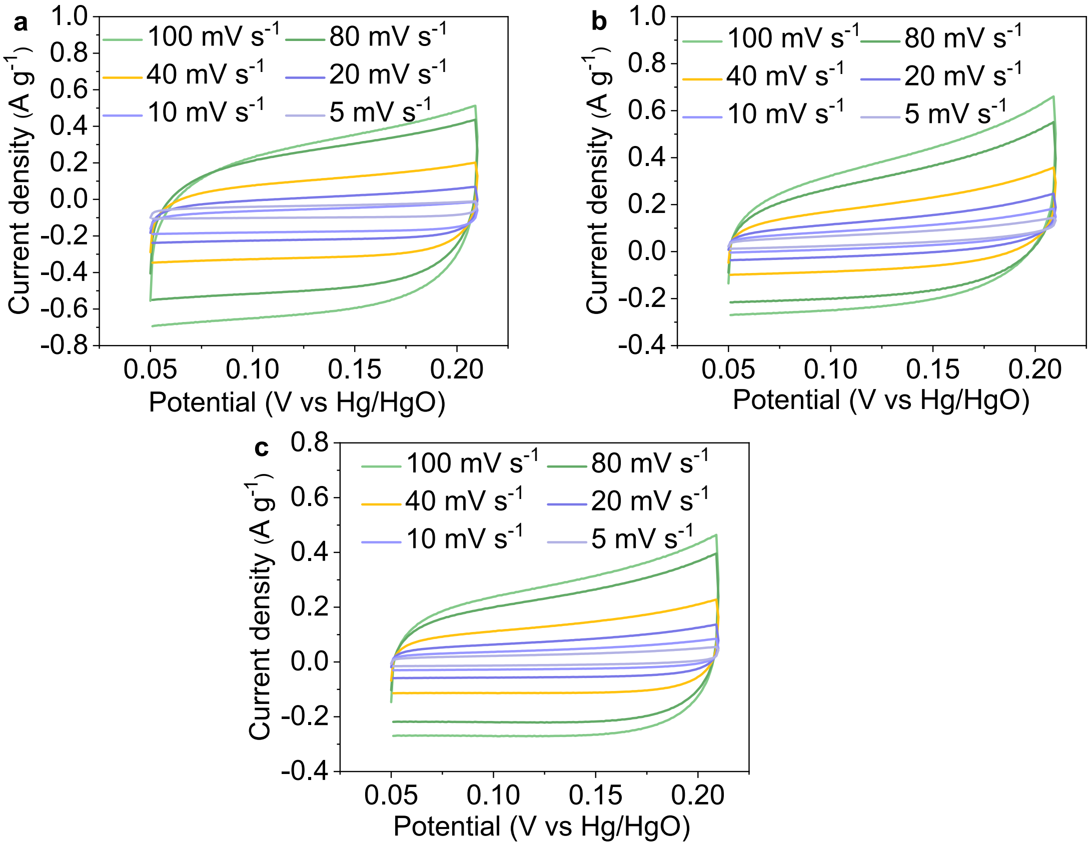

Fig. S10 CV curves at various current densities from 5 mV s^{-1} to 100 mV s^{-1} of (a) Mn-$Ni(OH)_2$@1T-MoS_2, (b) Mn-$Ni(OH)_2$/1T-MoS_2 and (c) Mn-$Ni(OH)_2$ electrodes in non-redox potential region (0.05 V - 0.21 V vs. Hg/HgO).

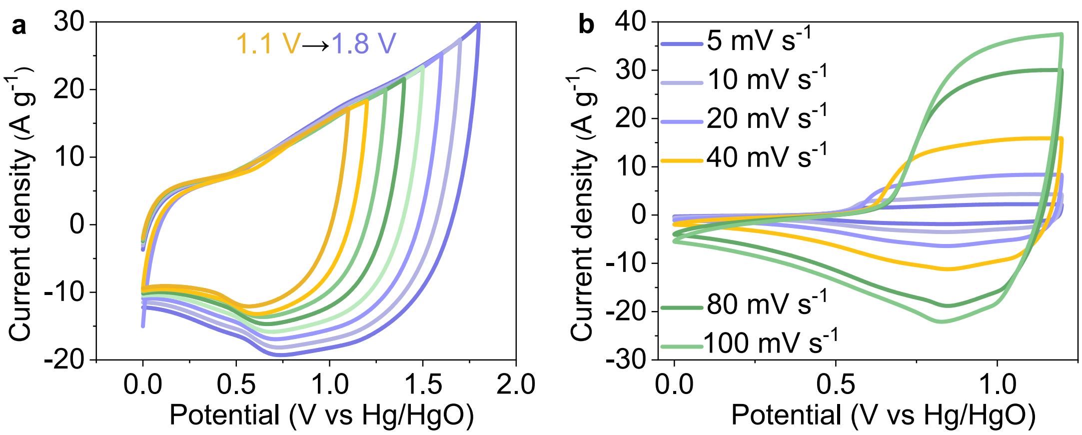

Fig. S11 CV curves at (a)various voltages from 1.1 V to 1.8 V and at (b) different scan rate from 5 mV s^{-1} to 100 mV s^{-1} of Mn-$Ni(OH)_2$@1T-MoS_2.

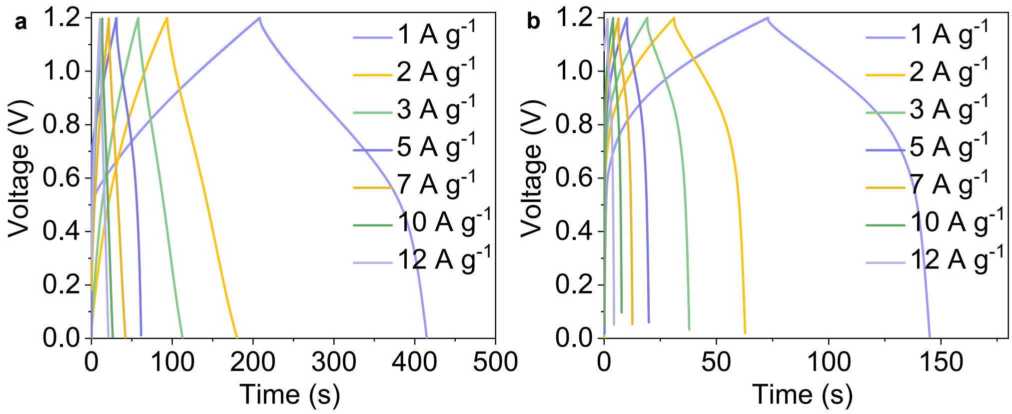

Fig. S12 GCD curves at various current densities from 1 A g^{-1} to 12 A g^{-1} of (a) Mn-$Ni(OH)_2$/1T-MoS_2//AC and (b) Mn-$Ni(OH)_2$//AC.

The specific capacity (C_A, mAh g^{-1}) was calculated using Equation S1 based on the discharge curve in GCD curves[1],

$$C_A = \frac{I \times \Delta t}{3.6 \times m} \qquad \text{Equation S1}$$

where I, m and Δt are the discharge current (A), the mass of active material (g) and the discharge time (s), respectively.

The relationship between the anodic peak currents (i) and scan rates (v) can be described by

$$i=av^b \qquad \text{Equation S3}$$

whrer a and b represent empirical parameters[2].

The ECSA of the electrode can be calculated according to Equation S2[3],

$$\mathrm{ECSA} = \mathrm{Cdl\ of\ electrode\ (mF\ cm^{-1})}/0.04\ \mathrm{(mF\ cm^{-1})} \qquad \text{Equation S3}$$

The ESR can be determined from a linear fit to the values for the IR_{drop} obtained from the GCD curves in Fig. S6 and Fig. 4d. This behavior is shown in Fig. 4e, according to Equation S3[4],

$$IR_{drop}=a+bI \qquad \text{Equation S4}$$

where a represents the difference between the applied potential and the charged potential of the capacitor, b represents double the ESR value.

The power density (P, W kg^{-1}) and energy density (E, Wh kg^{-1}) of the ASCs were calculated by Equation S4 and S5,

$$E = \frac{\mathrm{C_A} \times \Delta \mathrm{V}}{2} \qquad \text{Equation S5}$$

$$P = \frac{3600 \times E}{\Delta \mathrm{t}} \qquad \text{Equation S6}$$

where C_A, ΔV, Δt are the specific capacity (C_A, mAh g^{-1}), operating voltage (V) and discharge time (s) of the ASCs, respectively.

Table S1 The fitting values derived from the equivalent circuit using the Zview software.

Electrodes	**Mn-Ni(OH)$_2$@1T-MoS$_2$**	**Mn-Ni(OH)$_2$/1T-MoS$_2$**	**Mn-Ni(OH)$_2$**
R_s(Ω)	1.24	1.28	1.22
R_{ct}(Ω)	0.17	0.35	1.12
CPE1-T(Ω)	0.0030117	0.00043701	0.01452
CPE1-P(Ω)	0.86386	0.96999	0.668
R_2(Ω)	3247	2339	7883
CPE2-T(Ω)	0.001469	0.0017805	0.003137
CPE2-P(Ω)	0.89943	0.87256	0.90193

Table S2 Comparison of the electrochemical performance of $Ni(OH)_2$-based electrodes in a three-electrode system

Electrodes	**Electrolyte**	**Specific capacitance (mAh g^{-1})**	**Rate capability**	**Refs.**
Mn-$Ni(OH)_2$@1T-MoS_2	1M KOH	244.2(1 A g^{-1})	51.4%(1-12 A g^{-1})	This work
Mn-$Ni(OH)_2$/1T-MoS_2	1M KOH	112.2(1 A g^{-1})	43.1%(1-12 A g^{-1})	
Mn-$Ni(OH)_2$	1M KOH	70.4(1 A g^{-1})	39.2(1-12 A g^{-1})	
$Ni(OH)_2$@EG-DP	2M KOH	266(1 A g^{-1})	76%(1-20 A g^{-1})	5
$Ni(OH)_2$@NHCSs	2M KOH	214.8(1 A g^{-1})	51.7%(1-16 A g^{-1})	6
NiCo LDH/IPC	1M KOH	209.7(1 A g^{-1})	-	7
Co_3O_4@$Ni(OH)_2$	6M KOH	253.3(1 A g^{-1})	70.4%(1-20 A g^{-1})	8

Table S3 Comparison of electrochemical performance of $Ni(OH)_2$-based ACSs

Supercapacitors	**Energy density (Wh kg^{-1})**	**Power density (W kg^{-1})**	**Cycle number**	**Stability**	**Refs.**
MCMS-50 //$NiCo_2O_4$	48.96	600	10000	86.5% (10 A g^{-1})	9
NiMn-LDH/PC-1//AC	18.6	225.0	3000	58.2% (15 A g^{-1})	10
Co-Ni oxide-hydroxide//exfoliated graphite	5	416	2000	80% (2.5 mA cm^{-2})	11
$Ni(OH)_2$@EG-DP//AC	62.6	748.6	20000	84.5 % (8 A g^{-1})	5
$Ni(OH)_2$//active carbon	35.7	490	10,000	76% (100 mV s^{-1})	12
NiMn-LDH//AC	62.7	375.2	3000	100% (5 A g^{-1})	13
$Ni(OH)_2$@NHCSs‖NHCSs	37.5	800.0	10000	79.2% (8 A g^{-1})	6
NiCo LDH/IPC‖IPC	29.6	744	4000	88% (2 A g^{-1})	7
Co-CH@Ni-MOFs//AC	58.0	800.0	6000	80.7% (10 A g^{-1})	14
NiCo-LDH/rGO//CAC	49	401	2000	81% (2 A g^{-1})	15
Co_3O_4@$Ni(OH)_2$//AC	49.8	801.0	2000	93.0% (6 A g^{-1})	8
Ni_3S_2/Mn-doped $Ni(OH)_2$//AC-RGO	51.5	404.0	5000	85.3% (2.82 A g^{-1})	16
Co_3O_4@Mn-$Ni(OH)_2$/CC//AC	65.5	800.0	10000	93.0% (5 A g^{-1})	17
Mn-$Ni(OH)_2$@1T-MoS_2//AC	61.7	600	10000	72.7 % (5 A g^{-1})	This work
Mn-$Ni(OH)_2$/1T-MoS_2//AC	34.4	600	10000	13.8% (5 A g^{-1})	
Mn-$Ni(OH)_2$ //AC	12.0	600	10000	66.7% (5 A g^{-1})	

Reference

1. Q. Bi, Q. Ma, K. Tao and L. Han, *Dalton Trans.*, 2021, **50**, 8179-8188.
2. Y. Ma, L. Zhang, Z. Yan, B. Cheng, J. Yu and T. Liu, *Adv. Energy Mater.*, 2022, **12**, 2103820.
3. H. Liang, A. N. Gandi, D. H. Anjum, X. Wang, U. Schwingenschlogl and H. N. Alshareef, *Nano Lett.*, 2016, **16**, 7718-7725.
4. A. Izadi-Najafabadi, S. Yasuda, K. Kobashi, T. Yamada, D. N. Futaba, H. Hatori, M. Yumura, S. Iijima and K. Hata, *Adv. Mater.*, 2010, **22**, E235-E241.
5. Y. Huang, A. Buffa, H. Deng, S. Sarkar, Y. Ouyang, X. Jiao, Q. Hao and D. Mandler, *J. Power Sources*, 2019, **439**, 227046.
6. G. Wang, Z. Yan, Y. Ding, Z. Xu and Z. Li, *J. Colloid Interface Sci.*, 2022, **628**, 286-296.
7. X. Zhang, Q. Lu, E. Guo, J. Feng, M. Wei and J. Ma, *J. Energy Storage*, 2021, **38**, 102514.
8. X. Zhang, J. Xiao, X. Zhang, Y. Meng and D. Xiao, *Electrochim. Acta*, 2016, **191**, 758-766.
9. A. Mukherji, L. Saikia and R. Srivastava, *Chem. Eng. J.*, 2019, **373**, 1233-1246.
10. M. Yu, R. Liu, J. Liu, S. Li and Y. Ma, *Small*, 2017, **13**, 1702616.
11. P. G. Schiavi, P. Altimari, R. Zanoni and F. Pagnanelli, *J. Energy Chem.*, 2021, **58**, 336-344.
12. H. B. Li, M. H. Yu, F. X. Wang, P. Liu, Y. Liang, J. Xiao, C. X. Wang, Y. X. Tong and G. W. Yang, *Nat. Commun.*, 2013, **4**, 1894.
13. Z. Zhang, H. Huo, L. Wang, S. Lou, L. Xiang, B. Xie, Q. Wang, C. Du, J. Wang and G. Yin, *Chem. Eng. J.*, 2021, **412**, 128617.
14. X. Zhang, S. Yang, W. Lu, Y. Tian, Z. Liu, Y. Zhao and A. Liu, *Small*, 2022, **18**, e2200656.
15. L. Liu, A. R. Liu, Y. H. Xu, H. M. Yu, F. Q. Yang, J. Wang, Z. L. Zeng and S. G. Deng, *J. Mater. Res.*, 2020, **35**, 1205-1213.
16. L. Ye, Y. Zhou, Z. Bao, Y. Zhao, Y. Zou, L. Zhao and Q. Jiang, *J. Mater. Chem. A*, 2018, **6**, 19020-19029.
17. G. Wang, Y. Ding, Z. Xu, G. Wang, Z. Li and Z. Yan, *Chem. Eng. J.*, 2023, **469**, 143984.